Effects of synaptic conductance on the voltage distribution and firing rate of spiking neurons

Magnus J. E. Richardson*
Laboratory of Computational Neuroscience, Brain and Mind Institute, EPFL, CH 1015, Lausanne, Switzerland
(Received 1 December 2003; revised manuscript received 11 February 2004; published 28 May 2004)

A neuron in an active cortical circuit is subject to a fluctuating synaptic drive mediated by conductance changes. It was recently demonstrated that synaptic conductance effects *in vivo* significantly alter the integrative properties of neurons. These effects are missed in models that approximate the synaptic drive as a fluctuating current. Here the membrane-potential distribution and firing rate are derived for the integrate-and-fire neuron with δ correlated conductance-based synaptic input using the Fokker-Planck formalism. A number of different input scenarios are examined, including balanced drive and fluctuation changes at constant conductance, the latter of which corresponds to shifts in synchrony in the presynaptic population. This minimal model captures many experimentally observed conductance-related effects such as reduced membrane-potential fluctuations in response to increasing synaptic noise. The solvability of the model allows for a direct comparison with current-based approaches, providing a basis for assessing the validity of existing approximation schemes that have dealt with conductance change. In particular, a commonly used heuristic approach, whereby the passive membrane time constant is replaced by a drive-dependent effective time constant, is examined. It is demonstrated that this approximation is valid in the same limit that the underlying diffusion approximation holds, both for δ correlated as well as filtered synaptic drive.

DOI: 10.1103/PhysRevE.69.051918 PACS number(s): 87.19.La, 05.10.Gg, 05.40.−a, 87.10.+e

I. INTRODUCTION

Each neuron in the cortex receives thousands of inputs from other neurons via synaptic connections. The neuronal response to this synaptic input is a determining factor in action potential emission and can be accurately modeled using the conductance-based formalism of Hodgkin and Huxley in which the voltage dependence of the membrane currents is accounted for. However, the level of detail of this description comes at the expense of mathematical complexity and necessitates a numerical approach. Complementary to this is the study of simplified neuronal models that capture general features of neurons but also allow for an in-depth analysis. One such minimal model that has enjoyed a great deal of popularity is the integrate-and-fire (IF) neuron [1]. The degree of simplification underlying the IF model is compensated for by the wealth of derivable results: the model provides a framework against which the complex behavior of real neurons can be better examined.

One of the many simplifying assumptions of the standard IF neuron is the modeling of synaptic input as fixed charge injection. Real synapses, however, cause a transitory conductance increase through which a voltage-dependent current flows. The conductance changes in neurons subject to the massive synaptic bombardment *in vivo* have a significant effect on the neuronal response, including a reduced time constant [2,3] and suppression of fluctuations [4]. These properties in turn strongly affect spike emission, but are missed in the current-based model (hereafter referred to as IF_I).

A great deal of analytical work has been performed on neuronal models with synaptic reversal potentials since the 1960s. The bulk of this research concentrated on the moments of the interspike interval (ISI) distribution, first given analytically in Ref. [5]. A range of alternative models addressing the technical issue of the inhibitory boundary crossing were investigated [6]. Further work compared the ISI distributions with experiment [7,8], examined the effect of the postspike reset [9] and compared the coefficient of variation in the generated spike trains for different models [10]. Here the membrane-potential distribution in the presence of a threshold for spike generation and the firing rate are obtained analytically using the Fokker-Planck formalism. These results will be used to identify differences in the response of conductance and current-based models, as well as to evaluate an existing intermediate model. The Fokker-Planck approach is applicable to the study of the dynamics of both single neurons and populations of neurons in recurrent networks [11]. Hence, though it is the response of a single neuron that is examined here, the methods and results are applicable to the study of the collective states of populations of neurons with conductance-based synapses.

II. DEFINITION OF THE MODEL

The passive electrical properties of the neuron are modeled by a capacitance C in parallel with a leak current of conductance g_L (such that $C/g_L=\tau_L=20$ ms gives the passive time constant) that reverses at $E_L=-80$ mV (see Ref. [3]). The time evolution of the potential difference across the membrane V obeys

$$C\dot{V} = -g_L(V-E_L) - I_{syn}(t), \tag{1}$$

$$I_{syn}(t) = g_e(t)(V-E_e) + g_i(t)(V-E_i). \tag{2}$$

The synaptic current $I_{syn}(t)$ is comprised of both excitatory and inhibitory components which reverse at $E_e=0$ mV and

*Electronic address: Magnus.Richardson@epfl.ch

$E_i = -75$ mV with conductances $g_e(t)$ and $g_i(t)$ respectively. The excitatory conductance (with corresponding definitions for inhibition throughout the following section) is defined as

$$g_e(t) = Ca_e \sum_k \delta(t - t_k), \tag{3}$$

where a_e is a dimensionless measure of the strength of the synapse and the set $\{t_k\}$ counts over the Poisson-distributed times of all incoming excitatory pulses arriving at a total rate of $\mathcal{R}_e$. A single excitatory δ pulse is considered as the limit to zero width of a short pulse. An application of the usual conventions of calculus gives the jump of the membrane voltage from V to $V+\Delta V$ as

$$\Delta V = (E_e - V)(1 - e^{-a_e}). \tag{4}$$

It should be stressed that this update rule is different from a choice often made under similar situations: to multiply the δ functions by the value of the voltage just before the pulse arrival. Under those circumstances, the update rule given in Eq. (4) would be $\Delta V = (E_e - V)a_e$ instead. As it happens there is little practical difference between these two choices because $a_e \ll 1$. Nevertheless, it is the definition in Eq. (4) which is used here and will be seen later to lead to the *Stratonovich* formulation (see, for example, Ref. [12]) of the Fokker-Planck equation, rather than the *Itô* form.

The spike mechanism is implemented in the same way as other integrate-and-fire models: if the voltage reaches the spike threshold $V_{th} = -55$ mV it is immediately reset to $V_{re} = -65$ mV and a spike registered. This integrate-and-fire neuron with conductance-based synapses will be referred to as the IF_g model. The model appears to have been first defined in Ref. [5] (see [6] for alternative models) and can also be thought of as the limit of fast synaptic time constants in the model presented in Ref. [3].

In the results section the properties of the IF_g will be compared to a reference current-based IF_I model. This reference model is identical to that defined above except that for Eq. (4) the voltage dependence is replaced by a fixed reference voltage $V \to V_{ref}$ such that the IF_I and IF_g have postsynaptic potentials of the same amplitude at the reference voltage V_{ref}.

In all cases Monte Carlo simulations were implemented with δ pulse synaptic input [following the rule in Eq. (4)] and an integration time step of 1 μs. These δ pulse simulations allow for an assessment of the accuracy of the analytical results which are calculated in the diffusion approximation.

A. Method of solution

When the amplitudes a_e, a_i are small and the rates $\mathcal{R}_e, \mathcal{R}_i$ large, the diffusion approximation gives an accurate description of the dynamics. Heuristically, this corresponds to replacing Eq. (3) by

$$g_e(t) \simeq Ca_e[\mathcal{R}_e + \sqrt{\mathcal{R}_e}\xi_e(t),] \tag{5}$$

where ξ_e is a δ correlated Gaussian white-noise process $\langle \xi_e(t)\xi_e(t')\rangle = \delta(t-t')$. It is assumed here that the excitatory and inhibitory drive are uncorrelated. The resulting stochastic equation for the voltage yields the following Fokker-Planck (FP) equation

$$\tau \frac{\partial P}{\partial t} = \frac{1}{\gamma}\frac{\partial^2}{\partial V^2}[(V - E_S)^2 + E_D^2]P + \frac{\partial}{\partial V}(V - E)P \tag{6}$$

for the probability density $P(V,t)$ of finding a neuron with a voltage V at a time t. The method for deriving the FP equation for this case of multiplicative noise can be found in Ref. [12]. As was mentioned above in conjunction with the update rule specified in Eq. (4), it is the *Stratonovich* formulation that is used here.

The conservation of probability allows the writing of a continuity equation

$$\frac{\partial P}{\partial t} = -\frac{\partial J}{\partial V}, \tag{7}$$

where J is the probability current. Comparison of Eqs. (6) and (7) gives

$$-\tau J(V) = \frac{1}{\gamma}\frac{\partial}{\partial V}[(V - E_S)^2 + E_D^2]P + (V - E)P. \tag{8}$$

In this paper it is the steady-state properties that are examined, i.e., $\mathcal{R}_e$ and $\mathcal{R}_i$ do not vary over time. The current is therefore a piece-wise constant: below the reset V_{re} no current flows, between the reset and threshold V_{th} a constant current flows which is equal to the firing rate r:

$$J(V) = r\Theta(V - V_{re}), \tag{9}$$

where $\Theta(x)$ is the Heaviside or step function. The Eqs. (8) and (9) together can be solved to yield both $P(V)$ and r. However it is convenient to first introduce some new parameters. The synaptic conductance changes define an input-dependent time constant τ (not entirely a misnomer for steady Poissonian drive) and equilibrium potential E:

$$\tau^{-1} = \tau_L^{-1} + \mathcal{R}_e\tilde{a}_e + \mathcal{R}_i\tilde{a}_i, \tag{10}$$

$$E = \tau(E_L\tau_L^{-1} + \mathcal{R}_e\tilde{a}_eE_e + \mathcal{R}_i\tilde{a}_iE_i). \tag{11}$$

The shifted amplitude $\tilde{a}_e = (a_e - a_e^2/2)$ comes from the anomalous drift term of the *Stratonovich* formulation of the FP equation. If the *Itô* form were used then $\tilde{a}_e = a_e$. As already mentioned above, because $a_e \ll 1$ there is little practical difference between these formulations for the case of the model under examination in this paper.

Also introduced are two quantities with units of voltage:

$$E_S = (\mathcal{R}_e a_e^2 E_e + \mathcal{R}_i a_i^2 E_i)\chi, \tag{12}$$

$$E_D = (\mathcal{R}_e a_e^2 \mathcal{R}_i a_i^2)^{1/2}(E_e - E_i)\chi, \tag{13}$$

where $\chi = (R_e a_e^2 + R_i a_i^2)^{-1}$. The final parameter $\gamma = 2\chi/\tau$ is dimensionless and in the regime where the diffusion approximation is good $\gamma \gg 1$. The mean $\langle V\rangle$ and variance σ_V^2 in absence of threshold are calculated in terms of these parameters by taking moments of Eq. (6) yielding

$$\langle V\rangle = E \quad \text{and} \quad \sigma_V^2 = \frac{(E-E_S)^2 + E_D^2}{(\gamma - 1)}. \tag{14}$$

The spike mechanism is implemented by imposing $P(V_{th})=0$ and reinjecting the probability current (equal to the firing rate) flowing across V_{th} into V_{re}. A linear change in variables:

$$x = (V-E)\sqrt{\frac{\gamma}{(E-E_S)^2 + E_D^2}} \tag{15}$$

with x_{th} and x_{re} defined correspondingly, simplifies the following analysis. The steady-state FP equation for $f(x)dx = P(V)dV$ becomes

$$-r\tau\Theta(x-x_{re}) = \frac{d}{dx}(\alpha^2x^2 - 2\alpha\beta x + 1)f + xf, \tag{16}$$

where

$$\alpha = \frac{1}{\sqrt{\gamma}}, \quad \beta = \frac{(E_S - E)}{\sqrt{(E_S-E)^2 + E_D^2}} \tag{17}$$

and $\Theta(x)$ is the Heaviside or step function (the probability current flows only between x_{re} and x_{th}). The quantity β lies between $[-1,1]$: for pure excitation (when $\mathcal{R}_i=0$) $\beta=1$ and for pure inhibition (when $\mathcal{R}_e=0$) $\beta=-1$.

B. The voltage distribution and firing rate

Integration of Eq. (16) give the distribution $f(x)$ and firing rate r:

$$f = \frac{r\tau e^{-B(x)}}{(\alpha x-\beta)^2 + 1 - \beta^2}\int_x^{x_{th}} dy\Theta(y-x_{re})e^{B(y)}, \tag{18}$$

$$\frac{1}{r\tau} = \int_{-\infty}^{x_{th}} dx \int_x^{x_{th}} dy \frac{\Theta(y-x_{re})e^{-B(x)+B(y)}}{[(\alpha x-\beta)^2 + 1 - \beta^2]}. \tag{19}$$

Clearly the integral for the rate is best performed numerically by breaking the x integral into a part that factorizes $\{-\infty \ldots x_{re}\}$ and a finite part that does not $\{x_{re}\ldots x_{th}\}$. The function $B(x)$ is given by

$$B(x) = \frac{1}{2\alpha^2}\ln[(\alpha x-\beta)^2 + (1-\beta^2)] + \frac{\beta}{\alpha^2\sqrt{1-\beta^2}}\arctan\left(\frac{\alpha x\sqrt{1-\beta^2}}{1-\alpha\beta x}\right). \tag{20}$$

The freedom in offsetting $B(x)$ by a constant has been used to ensure that to leading order $B(x)\propto\alpha^0$, thus avoiding possible problems in the numerical integration of Eq. (19) for small α (large γ). The membrane-potential distribution [Eq. (18)] generalizes the results given in Ref. [13] in which the distribution in the absence of threshold was examined. It should also be noted that the firing rate in Eq. (19) is in agreement with the first moment of the ISI distribution found in Ref. [5] calculated using the first-passage time formalism.

III. THE SUBTHRESHOLD RESPONSE

First the subthreshold properties of the models with conductance and current-based synapses are contrasted. In Fig. 1 the responses of the synaptically active IF_g and IF_I neurons to step current injection are displayed. Both neurons receive an identical synaptic input with postsynaptic potentials that are of equal amplitude at the initial mean voltage of −65 mV (V_{ref} in the definition of the IF_I is −65 mV). After the onset of the step current at 100 ms the mean voltages of the two models exponentially relax to their new values. For the IF_g the response is quick with a time constant of $\tau=5$ ms, whereas, the IF_I responds more slowly with the passive time constant of $\tau_L=20$ ms. The statistics of the fluctuations about the mean voltages can also be contrasted. The standard deviations of the fluctuations about the mean are 1 and 2 mV for the IF_g and IF_I, respectively. The relative suppression of fluctuations by a factor $\sqrt{\tau/\tau_L}$ is another consequence of the synaptic conductance increase. This suppressed response to input is also manifested in the shift of the mean voltage due to the step-current injection. The induced change is only 1 mV for the IF_g but is 4 mV for the IF_I The decreased response is proportional to the conductance ratio which, written in the terms of the time constants, is τ/τ_L.

This simple example demonstrates that the IF_g model comprising δ pulse conductance-based synapses captures many of the response properties to synaptic drive missed by the IF_I model, including reduced membrane fluctuations, a shortened time constant and suppressed response to injected current.

Anomalous effect of presynaptic noise

An increase in the presynaptic drive causes both a conductance increase as well as an increase in the synaptic noise, or fluctuations and can lead to qualitatively new behavior for the IF_g model. A scenario is considered in which excitatory and inhibitory input rates are increased in a balanced way, such that the equilibrium potential E remains constant. Using Eqs. (10) and (11) the relation between the excitatory and inhibitory rates can be obtained

$$(E-E_L)/\tau_L + (E-E_e)\mathcal{R}_e\tilde{a}_e + (E-E_i)\mathcal{R}_i\tilde{a}_i = 0, \tag{21}$$

where the condition of positivity requires that

$$R_e \geqslant \left(\frac{E-E_L}{E_e-E}\right)\frac{1}{\tilde{a}_e\tau_L}. \tag{22}$$

An increase of both $\mathcal{R}_e$ and $\mathcal{R}_i$ subject to Eq. (21) leads to an increase in synaptic noise [see Eq. (5)]. However, the concomitant increase in the total conductance [a decrease in τ, see Eq. (10)] acts to suppress voltage fluctuations: the two effects are in competition. In Fig. 2 the standard deviation σ_V of the membrane potential is plotted against this balanced increasing drive for different fixed E. At depolarized values increased synaptic rates lead to increased voltage fluctuations. However, at hyperpolarized potentials the conductance increase from the inhibitory drive is stronger and the effect reverses: increased synaptic fluctuations lead to *decreased* voltage fluctuations.

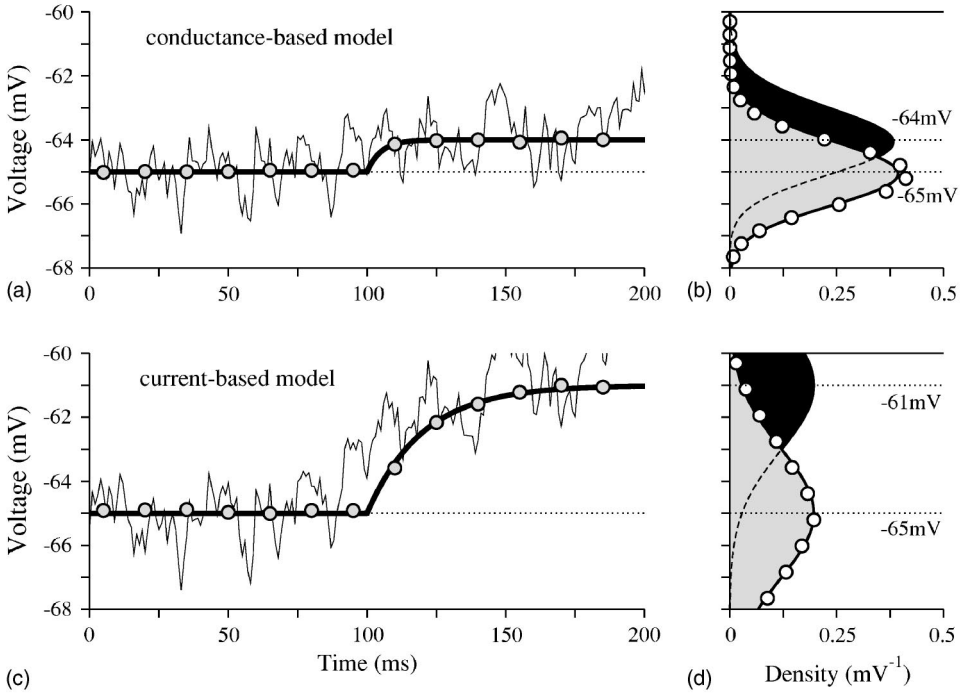

FIG. 1. Comparison of the IF_g and IF_I models of conductance and current-based synaptic drive. Synaptic input is at a rate $\mathcal{R}_e=15.0$ and $\mathcal{R}_i=9.23$ kHz. The IF_g has postsynaptic potentials (PSPs) with voltage-dependent amplitude, whereas those of the IF_I are fixed such that at the initial equilibrium voltage of −65 mV both models have PSPs with amplitudes of 0.13 mV ($\tilde{a}_e=0.002, \tilde{a}_i=0.013$). In panels a and c the response to a step current of magnitude $I_{step}/C=0.2$ nA/nF with onset at 100 ms is plotted: (−) example time courses (with identical spike-train inputs) of the voltage V, (−) mean voltage, (∘) simulations. (a) The mean voltage in the IF_g shifts by 1 mV, with a time constant of $\tau=5$ ms. (c) The shift for the IF_I is 4 mV with a time constant of $\tau_L=20$ ms. Panels (b) and (d): the voltage distributions before (gray) and long after (black) the onset of the step current. The standard deviation of the IF_g model is 1.0 mV whereas for the IF_I it is 2.0 mV.

The two variances, first, when $\mathcal{R}_i=0$ [the equality in Eq. (22)] and secondly in the limit of large rates $\mathcal{R}_e, \mathcal{R}_i \to \infty$:

$$\mathcal{R}_i \simeq \mathcal{R}_e \left(\frac{\tilde{a}_e(E-E_e)}{\tilde{a}_i(E-E_i)} \right), \tag{23}$$

can be compared to find at which value of $\langle V \rangle = E^*$ the effect of synaptic fluctuations reverses. Noting that for the present case $a_e(E_i-E_L) \ll a_i(E_e-E_L)$ the point at which noise increase and conductance increase balance is

$$E^* \simeq E_i \left(1 - \sqrt{\frac{a_e(E_i-E_L)}{a_i(E_e-E_L)}} \right). \tag{24}$$

This yields a value near −68 mV for the case in Fig. 2. This behavior should be contrasted with that of the IF_I model for which the standard deviation always grows with synaptic fluctuations as $\sqrt{R_{e,i}}$.

The suppression of fluctuations due to conductance increase has been seen *in vivo* [4]. It should be noted that the effect shown in Fig. 2 is also mirrored in the statistics of the fluctuating equilibrium potential $E(t)$ that was analyzed in Ref. [14]. However, the input-dependent filtering due to the effective membrane time constant [Eq. (10)] must be taken into account to fully quantify the effect on the voltage standard deviation, as was done here. The decrease in voltage fluctuations with increasing synaptic noise has been shown to lead to a decreasing firing rate in simulations of the Hodgkin-Huxley model [15]. With the present choice of parameters it appears that the effect is at too hyperpolarized potentials to impact significantly on spike emission.

IV. THE FIRING-RATE RESPONSE

A. Firing due to depolarizing synaptic drive

One way in which the firing rate of a neuron can be increased is by shifting the equilibrium potential E to more depolarized values. This is achievable through either (i) increasing the excitatory drive, (ii) a combination of increasing excitation and decreasing inhibition, or (iii) decreasing inhibition only. In Fig. 3(a) these cases are plotted. For the IF_I model under similar circumstances the firing rate would be expected to grow linearly with E for strong drive. A similar response is seen for case (ii) where a balanced input has been chosen such that the conductance remains constant (τ fixed at 6 ms for all E). For case (i) the increasing excitatory rate leads to a shortened time constant and a faster increase in the firing rate with E such that $r_i(E)/r_{ii}(E) \propto (E_e-E)^{-1}$. For case (iii), however, the reverse effect is seen due to the decreasing inhibitory rate and increasing time constant: in this case $r_{iii}(E)/r_{ii}(E) \propto (E-E_i)^{-1}$.

B. Firing due to increased voltage fluctuations

An increase of membrane-potential fluctuations will tend to increase the firing rate of neurons. Two such scenarios are

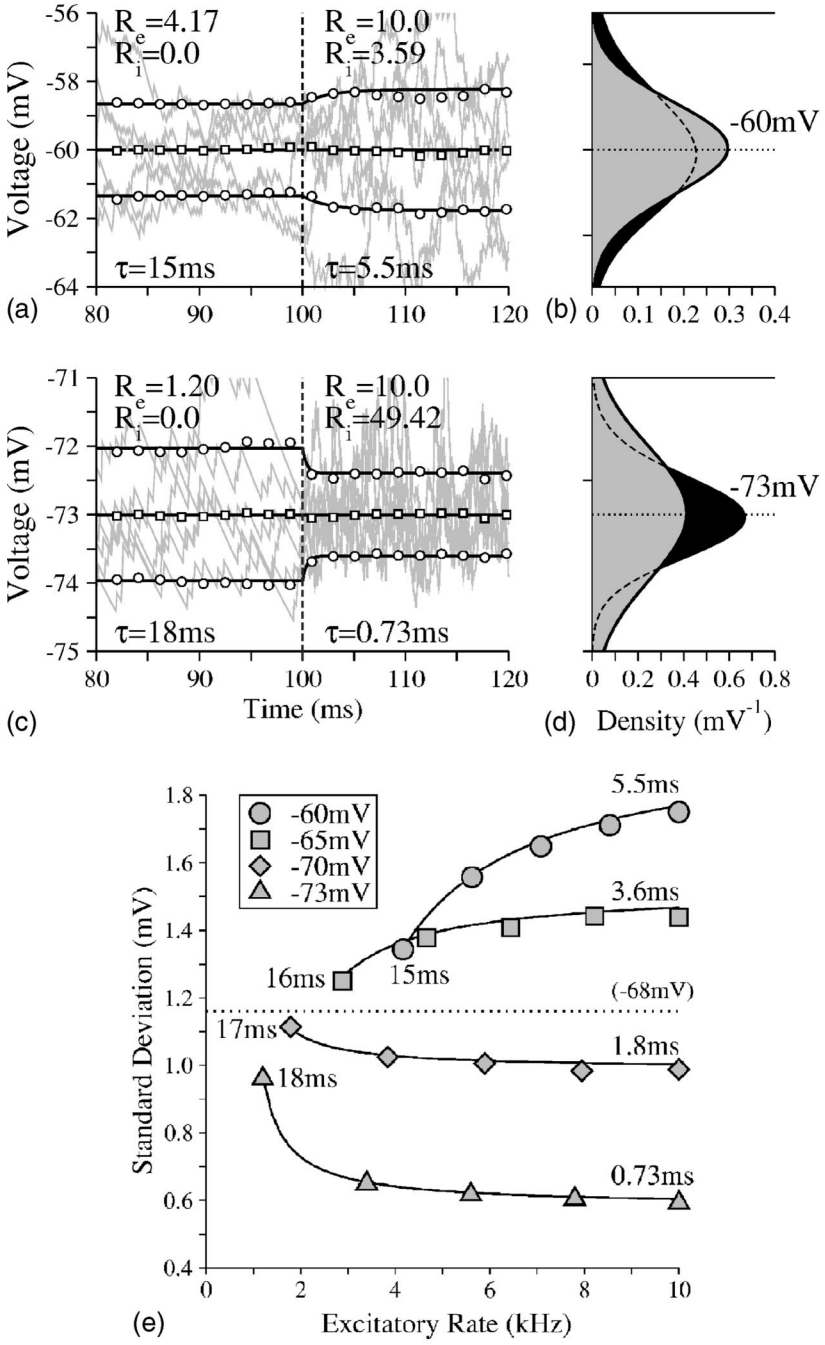

FIG. 2. Response of the conductance-based synapses model IF_g to balanced changes [see Eq. (21)] in the presynaptic rates: a demonstration of the competing effects of synaptic fluctuations and synaptic conductance increase. (a) A balanced step change (at 100 ms) in the incoming rates (given in kHz the panel) with E held constant at −60 mV. At depolarized potentials an increased synaptic drive leads to an increase in the standard deviation from 1.35 to 1.77 mV: the fluctuation increase dominates over the conductance increase. (b) The membrane voltage distributions before (gray) and long after (black) the change in synaptic drive. A weak skew in the distributions is visible. (c) A balanced step change in the incoming rates (given in the panel) with E held constant at −73 mV. At hyperpolarized potentials the increasing synaptic drive leads to a *decrease* in the standard deviation from 0.97 to 0.60 mV: the conductance increase dominates over the increase in synaptic fluctuations. (d) The effect is seen in a sharpening of the distribution from before (gray) to after (black) the step change. In both panels (a) and (c) a number of example trajectories have been plotted in gray and the membrane time scales given before and after the step change. (e) The standard deviation as a function of increasing fluctuations (balanced synaptic drive parameterized by $\mathcal{R}_e$) for different values of fixed E given in the legend. The initial point in each curve corresponds to $\mathcal{R}_i=0$ and the final to $\mathcal{R}_e=10$ kHz. The time labels give the values of τ at these points (the inverse of which are related to the total conductance). The examples given in panels (a) and (c) can be identified on panel (e). The effect of increasing synaptic drive reverses at a mean membrane voltage of $E^* \simeq -68$ mV [see Eq. (24)]. In all cases $\tilde{a}_e=0.004$ and $\tilde{a}_i=0.026$ giving postsynaptic potentials of size $\simeq 0.26$ mV at −65 mV. Simulational data are denoted by symbols.

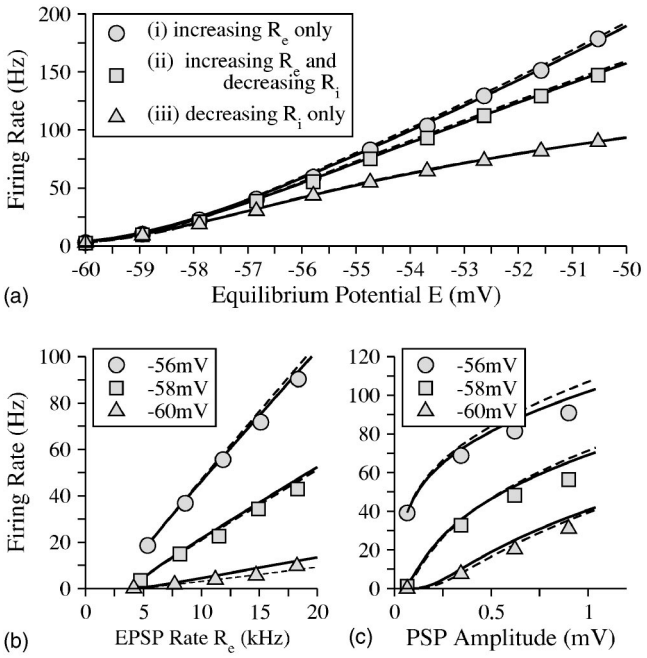

FIG. 3. (a) Firing rate with increasing equilibrium potential E. The initial values of $\mathcal{R}_e=9.17$ and $\mathcal{R}_i=3.08$ kHz give $E=-60$ mV and a time constant of 6 ms. The equilibrium potential E is then increased through three different mechanisms (see legend and text). (b) Firing-rate curves for balanced synaptic input (at fixed E given in the legend) as a function of increasing presynaptic noise parametrized by $\mathcal{R}_e$. (c) Firing rate curves at constant conductance (both E and $\tau=5$ ms fixed) as a function of increasing synaptic noise parameterized by the postsynaptic potential (PSP) size. This scenario corresponds to an increase in presynaptic synchrony and is achieved by keeping the products $\mathcal{R}_e\tilde{a}_e$ and $\mathcal{R}_i\tilde{a}_i$ fixed while $\tilde{a}_e$ and $\tilde{a}_i$ are varied. Here the EPSPs and IPSPs amplitudes are identical at -65 mV and provide the abscissa of the plot. The range of PSPs for which the diffusion approximation is valid is seen in the fit with simulations. In all figures the bold lines are the firing rate Eq. (19) and the broken lines a current-based approximation accounting for the tonic conductance increase (see text). For panels (a) and (b) $\tilde{a}_e=0.004$ and $\tilde{a}_i=0.026$.

considered, the first is equivalent to the balanced input described above in Eq. (21) and Fig. 2. In Fig. 3(b) the linearity of the firing rate for this case can be understood because the parameters α and β in Eq. (19) saturate with large $\mathcal{R}_e,\mathcal{R}_i$ and because the prefactor τ^{-1} of the rate [Eq. (19)] grows linearly with $\mathcal{R}_e$. This should be contrasted with the response of the $\mathrm{IF_I}$ model to the same input for which the firing rate would grow in proportion to $\sqrt{\mathcal{R}_{e,i}}$.

For the second mode of increasing fluctuations considered both E and τ are held constant (constant conductance). This is achieved by fixing

$$\mathcal{R}_e\tilde{a}_e=\frac{1}{(E_e-E_i)}\left(\frac{1}{\tau}(E-E_i)+\frac{1}{\tau_L}(E_i-E_L)\right),$$

$$\mathcal{R}_i\tilde{a}_i=\frac{1}{(E_e-E_i)}\left(\frac{1}{\tau}(E_e-E)-\frac{1}{\tau_L}(E_e-E_L)\right), \qquad (25)$$

and increasing $\tilde{a}_e,\tilde{a}_i$ whilst decreasing $\mathcal{R}_e,\mathcal{R}_i$. It can be thought of as a crude model of changing synchrony in the presynaptic population (for a more sophisticated treatment for the $\mathrm{IF_I}$ model see Ref. [16]). This mode of firing, in which the variance changes but the mean drive remains constant, is the conductance-based-drive analog to the scenario discussed in Ref. [17] in the context of fast signaling. The increasing firing rate of the neuron in response to increased synchrony is plotted in Fig. 3(c) against the amplitude of the postsynaptic potentials (PSPs).

These different effects, which are missed in current-based models of synaptic noise, provide the mechanisms for the neuronal gain modulation seen recently in experiment [18].

V. CONCLUSION

The results presented above demonstrate that the modeled response of neurons is qualitatively different when conductance effects are taken into account. So must all previous results derived using the $\mathrm{IF_I}$ model be discarded?

One approach to dealing with conductance-based input has been to use the current-based $\mathrm{IF_I}$ framework with an input-dependent time constant (see Ref. [19] for a recent treatment). This corresponds to taking into account the tonic conductance change and the fluctuations in the current component of the synaptic input, but ignoring the fluctuations in the conductance component of the synaptic drive:

$$g_e(V-E_e)=g_{e0}(V-E_e)+g_{e,fluct}(V-E_e)$$
$$\simeq g_{e0}(V-E_e)+g_{e,fluct}(\langle V\rangle-E_e)+\cdots. \qquad (26)$$

The approximation is valid because the voltage fluctuations $\delta V=V-\langle V\rangle$ scale with $g_{e,fluct}$ and therefore the higher-order fluctuations $g_{e,fluct}\delta V$ in the synaptic drive are of secondary importance.

The subthreshold probability density found in Ref. [19] under such an approximation scheme can be shown to satisfy the Fokker-Planck Eq. (16) with $\alpha=0$. This zero-order solution in the α expansion of Eq. (16) is equivalent to a *Gaussian approximation*. In this approximation the diffusion constant of the Fokker-Planck equation becomes voltage-independent, reflecting the fact that the fluctuations in the effective time constant have been neglected. What is important to note is that the small α, or large γ, limit is also the limit in which the underlying diffusion approximation is valid. Hence one expects this approximation to be accurate in the same limit. Though care needs to be taken when the width of the distribution is strongly affected by the threshold and reset, generally speaking the approximation is excellent. A comparison of the bold (full solution) and broken (effective-time-constant or Gaussian approximation) lines in Fig. 3 shows that the approximation is valid in all cases, except for when the postsynaptic potentials are relatively large [Fig. 3(c)]. This is as expected because it is here also that the diffusion approximation begins to break down.

These arguments can be extended to the more biologically realistic case of synaptic filtering arising from the exponential decay of the synaptic pulse. It has been shown [20,21]

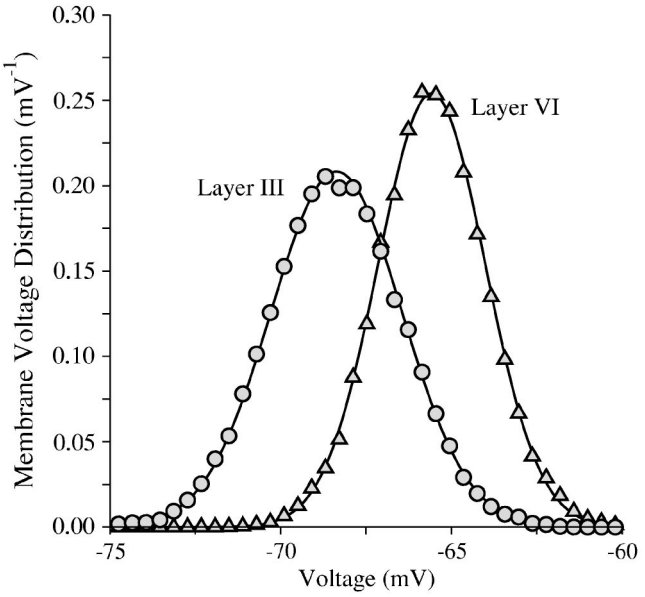

FIG. 4. The subthreshold voltage distribution corresponding to models of filtered synaptic input to layer III (circles) and layer VI (triangles) cortical neurons. The symbols correspond to a Monte Carlo simulation of a passive membrane [defined by Eq. (2)] receiving excitatory and inhibitory filtered synaptic input of the form given in Eq. (27). The lines correspond to the Gaussian, or effective-time-constant approximation defined by the moments given in Eqs. (30) and (33). The passive membrane parameters are defined in the text (with $C=1\ \mu\mathrm{F/cm^2}$) and parameters of the synaptic drive for the two models were taken from Ref. [3]: the layer III neuron $\{g_{e0}=0.0295, g_{i0}=0.217, \sigma_e=0.00935, \sigma_i=0.034, \tau_e=7.8, \tau_i=8.8\}$ and the layer VI neuron $\{g_{e0}=0.0346, g_{i0}=0.165, \sigma_e=0.00866, \sigma_i=0.0191, \tau_e=2.7, \tau_i=10.5\}$. The conductances are in units of $\mathrm{mS/cm^2}$ and the time constants in milliseconds.

for the $\mathrm{IF_I}$ model that neurons subject to temporally correlated synaptic input have a different high-frequency response as compared to those subject to white-noise drive. Furthermore, models of conductance-based synaptic drive with temporal correlations exhibit voltage fluctuations with the same statistics [2,3] as those seen *in vivo*. The form of the filtered synaptic input (using the excitatory drive as an example) given in Ref. [3] is

$$\tau_e \dot{g}_e = g_{e0} - g_e + \sigma_e \sqrt{2\tau_e}\,\xi_e(t), \tag{27}$$

where τ_e is the filtering constant, g_{e0} the tonic conductance, σ_e the standard deviation of the conductance fluctuations and $\xi_e(t)$ is a δ correlated white-noise process of unit variance. The effective-time-constant approximation in this case corresponds to the following equation for the voltage:

$$\tau_0 \dot{V} = -(V-E_0) - u_e(t)(E_0-E_e) - u_i(t)(E_0-E_i), \tag{28}$$

where the conductance change has been absorbed into a drive-dependent membrane time constant

$$\tau_0 = \frac{C}{g_L + g_{e0} + g_{i0}} \tag{29}$$

with the average voltage $\langle V\rangle = E_0$ given by

$$E_0 = \frac{g_L E_L + g_{e0}E_e + g_{i0}E_i}{g_L + g_{e0} + g_{i0}}, \tag{30}$$

and the fluctuating part given by

$$u_e(t) = \left(\frac{\sigma_e \tau_0}{C}\right) \int_{-\infty}^{t} \frac{ds}{\tau_e} e^{-(t-s)/\tau_e} \sqrt{2\tau_e}\,\xi_e(s). \tag{31}$$

Written in this form, it is clear that the voltage in Eq. (28) is a Gaussian random variable. The variance can be calculated in terms of the small parameters

$$\epsilon_e^2 = \left(\frac{\tau_e}{\tau_0+\tau_e}\right)\left(\frac{\sigma_e\tau_0}{C}\right)^2, \quad \epsilon_i^2 = \left(\frac{\tau_i}{\tau_0+\tau_i}\right)\left(\frac{\sigma_i\tau_0}{C}\right)^2 \tag{32}$$

and shown to take the particularly simple form

$$\langle (V-E_0)^2\rangle = \epsilon_e^2 (E_0-E_e)^2 + \epsilon_i^2 (E_0-E_i)^2. \tag{33}$$

This result differs from that obtained in Ref. [22] in which an approach using the *Itô* calculus was presented.

The equations for the mean (30) and the variance (33) can be calculated more systematically from either an expansion of the full solution to Eqs. (2) and (27):

$$V(t) = \int_{-\infty}^{t} \frac{ds}{C} [g_L E_L + g_e(s)E_e + g_i(s)E_i] e^{-\int_s^t [dr/\tau(r)]}, \tag{34}$$

where $\tau(r) = C/[g_L + g_e(r) + g_i(r)]$, or by taking moments of the corresponding three-variable Fokker-Planck equation:

$$\begin{aligned}\frac{dP}{dt} = {} & \frac{1}{C}\frac{\partial}{\partial V}[g_L(V-E_L) + g_e(V-E_e) + g_i(V-E_i)]P \\ & + \frac{\sigma_e^2}{\tau_e}\frac{\partial^2}{\partial g_e^2}P + \frac{1}{\tau_e}\frac{\partial}{\partial g_e}(g_e - g_{e0})P + \frac{\sigma_i^2}{\tau_i}\frac{\partial^2}{\partial g_i^2}P \\ & + \frac{1}{\tau_i}\frac{\partial}{\partial g_i}(g_i - g_{i0})P.\end{aligned} \tag{35}$$

Such results agree, to leading order, with the Gaussian or effective-time-constant approximation. Comparisons of this approximation for the voltage distribution with simulations are presented in Fig. 4.

In summary, a number of analytical results were derived for the integrate-and-fire neuron with both δ pulse and filtered conductance-based synapses. These results allowed

for a comparison to be made between the mathematical structures of conductance and current-based models. It was demonstrated that a current-based model with a drive-dependent time constant provides a simple and accurate description of biologically relevant models of neuronal response to conductance-based synaptic input.

ACKNOWLEDGMENTS

I thank Wulfram Gerstner for his support for this project. I would also like to thank Petr Lansky for useful discussions on the existing analytical work on synaptic drive, as well as Nicolas Brunel and Vincent Hakim for their constructive comments on a previous version of this paper.

[1] R. B. Stein, Biophys. J. **5**, 173 (1965).
[2] A. Destexhe and D. Paré, J. Neurophysiol. **81**, 1531 (1999).
[3] A. Destexhe, M. Rudolph, J.-M. Fellous, and T. J. Sejnowski, Neuroscience **107**, 13 (2001).
[4] C. Monier, F. Chavane, P. Baudot, L. J. Graham, and Y. Frégnac, Neuron **37**, 663 (2003).
[5] P. I. M. Johannesma, in *Neural Networks*, edited by ER Caianiello (Springer, New York, 1968), pp. 116–144.
[6] P. Lansky and V. Lanska, Biol. Cybern. **56**, 19 (1987).
[7] H. C. Tuckwell, J. Theor. Biol. **77**, 65 (1979).
[8] W. J. Wilbur and J. Rinzel, J. Theor. Biol. **105**, 345 (1983).
[9] P. Lansky and M. Musila, Biol. Cybern. **64**, 285 (1991).
[10] M. Musila and P. Lansky, J. Theor. Biol. **171**, 225 (1994).
[11] N. Brunel and V. Hakim, Neural Comput. **11**, 1621 (1999).
[12] H. Risken, *The Fokker-Planck Equation* (Springer-Verlag, Berlin, 1996).
[13] V. Lanska, P. Lansky, and C. E. Smith, J. Theor. Biol. **166**, 393 (1994).
[14] S. Stroeve and S. Gielen, Neural Comput. **13**, 2005 (2001).
[15] P. H.E. Tiesinga, J. V. José, and T. J. Sejnowski, Phys. Rev. E **62**, 8413 (2000).
[16] R. Moreno, J. de la Rocha, A. Renart, and N. Parga, Phys. Rev. Lett. **89**, 288101 (2002).
[17] G. Silberberg, M. Bethge, H. Markram, K. Pawelzik, and M. Tsodyks, J. Neurophysiol. **91**, 704 (2004).
[18] F. S. Chance, L. F. Abbott, and A. D. Reyes, Neuron **35**, 773 (2002).
[19] A. N. Burkitt, Biol. Cybern. **85**, 247 (2001).
[20] N. Brunel, F. S. Chance, N. Fourcaud, L. F. Abbott, Phys. Rev. Lett. **86**, 2186 (2001).
[21] N. Fourcaud and N. Brunel, Neural Comput. **14**, 2057 (2002).
[22] M. Rudolph and A. Destexhe, Neural Comput. **15**, 2577 (2003).